

# Au plasmonics in a $\text{WS}_2\text{-Au-CuInS}_2$ photocatalyst for significantly enhanced hydrogen generation

Zhongzhou Cheng, Zhenxing Wang<sup>\*</sup>, Tofik Ahmed Shifa, Fengmei Wang, Xueying Zhan, Kai Xu, Quanlin Liu, and Jun He<sup>\*</sup>

Citation: *Appl. Phys. Lett.* **107**, 223902 (2015); doi: 10.1063/1.4937008

View online: <http://dx.doi.org/10.1063/1.4937008>

View Table of Contents: <http://aip.scitation.org/toc/apl/107/22>

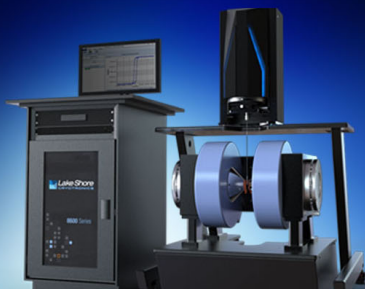
Published by the [American Institute of Physics](#)

---

---




Lake Shore  
CRYOTRONICS



**NEW 8600 Series VSM**

For fast, highly sensitive  
measurement performance

LEARN MORE 

# Au plasmonics in a WS<sub>2</sub>-Au-CuInS<sub>2</sub> photocatalyst for significantly enhanced hydrogen generation

Zhongzhou Cheng,<sup>1,2</sup> Zhenxing Wang,<sup>1,a)</sup> Tofik Ahmed Shifa,<sup>1</sup> Fengmei Wang,<sup>1</sup> Xueying Zhan,<sup>1</sup> Kai Xu,<sup>1</sup> Quanlin Liu,<sup>2</sup> and Jun He<sup>1,a)</sup>

<sup>1</sup>CAS Key Laboratory of Nanosystem and Hierarchical Fabrication, National Center for Nanoscience and Technology, Beijing 100190, China

<sup>2</sup>School of Materials Science and Engineering, University of Science and Technology Beijing, Beijing 100083, China

(Received 8 September 2015; accepted 22 November 2015; published online 2 December 2015)

Promoting the activities of photocatalysts is still the critical challenge in H<sub>2</sub> generation area. Here, a Au plasmon enhanced photocatalyst of WS<sub>2</sub>-Au-CuInS<sub>2</sub> is developed by inserting Au nanoparticles between WS<sub>2</sub> nanotubes and CuInS<sub>2</sub> (CIS) nanoparticles. Due to the localized surface plasmonic resonance properties from Au nanoparticles, WS<sub>2</sub>-Au-CIS shows the best performance as compared to Au-CIS, CIS, WS<sub>2</sub>-CIS, CIS-Au, WS<sub>2</sub>-Au, and WS<sub>2</sub>-CIS-Au. The surface plasmonic resonance effects dramatically intensify the absorption of visible light and help to inject hot electrons into the semiconductors. Our findings open up an efficient method to optimize the type-II structures for photocatalytic water splitting. © 2015 AIP Publishing LLC. [<http://dx.doi.org/10.1063/1.4937008>]

Aiming at visible light active photocatalysts, the design of heterogeneous semiconductors has been widely regarded as one of the most promising routes.<sup>1</sup> Compared with single component photocatalysts (TiO<sub>2</sub>, ZnO, etc.),<sup>2</sup> composite photocatalysts with suitable band gaps and matched edge positions usually exhibit higher performance. They own different electronic energy levels that enable electron-hole faster separation and less recombination.<sup>3–7</sup> To prevent the recombination of the photogenerated carriers, an efficient method is to utilize heterogeneous architecture with type-II band alignment.<sup>8,9</sup> Notably, as part of such constituents, extensive investigations<sup>10–12</sup> were made on transition metal dichalcogenides (TMDs) by virtue of their potential use as electrodes for electrochemical solar energy conversion because of following points. (I): Their appropriate band gaps (1.1–1.7 eV) closely match to the solar spectrum. (II): The photon absorption in layered TMDs involves d-d transition which does not result in breaking of chemical bonds, unlike those in CdS, involving p-s transition that suffers from photodecomposition.<sup>13</sup> In category of TMDs, WS<sub>2</sub> is an attractive material for the solar energy conversion because it combines a narrow band gap and a chemical inertness over a fair pH range.<sup>14–17</sup> In line with this, we have recently achieved WS<sub>2</sub> nanotubes (NTs) and controllably derived WS<sub>2(1-x)</sub>Se<sub>2x</sub> NTs on flexible and conductive carbon fiber (CF) substrate.<sup>18</sup>

Additionally, owing to its high absorption coefficient and ideal band gap (~1.4 eV),<sup>19</sup> copper indium sulfide (CuInS<sub>2</sub>, CIS) has demonstrated fruitful results in solar cell technology and reported to be a shallow absorber in the visible region.<sup>20–22</sup> Meanwhile, it has also become known for being promising alternative to the toxic light absorbing materials currently in use.<sup>23–25</sup> However, it exhibits low activity for water reduction<sup>26</sup> arising from fast carrier recombination which is detrimental to split water. One possible method to improve the carrier separation rate and reduce the recombination rate is to

construct heterostructures with type II band alignments. However, for WS<sub>2</sub>/CIS type II photocatalyst, photogenerated electron tends to transfer from the conduction band of CIS to that of WS<sub>2</sub>, which results in the lower hydrogen production efficiency than individual CIS photocatalyst.

Herein, we constructed a plasmon enhanced composite photocatalyst by inserting Au nanoparticles between WS<sub>2</sub> and CIS for high efficiency hydrogen evolutions. The incorporation of noble-metal Au nanoparticles can introduce a new phenomenon<sup>27</sup> that enables the electrons to be densely available onto the conduction band of CIS. This is due to the fact that the noble-metal nanoparticles can employ their extraordinary surface plasmonic resonance (SPR) properties to inject hot electrons to the semiconductors.<sup>28</sup> This ensures the accessibility of plenty of electrons on the conduction band of CIS. The photoelectrochemical (PEC) performances as well as hydrogen generation activities of the samples were carefully investigated. WS<sub>2</sub>-Au-CIS photocatalyst shows the best performance, which is attributed to SPR effects of Au nanoparticles. Our findings may open up an efficient method to further improve the photocatalytic activities of type II composite nanostructures.

The samples were prepared in a three-step process. First, WO<sub>3</sub> nanowires were grown on a CF substrate followed by sulfurization to get WS<sub>2</sub> nanotube using CVD method.<sup>18,29</sup> Second, the prepared WS<sub>2</sub> nanotubes on CF were immersed in the solution containing Au nanoparticles with a uniform diameter of 20 nm for 30 min.<sup>30</sup> Finally, the CIS nanoparticles were electroplated on the dry WS<sub>2</sub>-Au system with an impulse current.<sup>31,32</sup> All the samples were annealed in Ar at 450 °C for 2 h.

The crystal structure, morphology, and chemical composition of the composites were analyzed with X-ray diffraction (XRD, D/MAX-TTRIII(CBO) diffractometer using Cu-K $\alpha$  radiation ( $\lambda = 1.5418 \text{ \AA}$ ), field emission scanning electron microscopy (FE-SEM, Hitachi S4800), and field emission transmission electron microscopy (FE-TEM, Tecnai G2 F 20) with energy dispersive X-ray (EDX) spectroscopy, respectively. Raman spectra of the samples were obtained using an

<sup>a)</sup> Authors to whom correspondence should be addressed. Electronic addresses: wangzx@nanoctr.cn and hej@nanoctr.cn

InVoRENISHAW system. The light absorption spectra were measured using UV/vis/NIR spectrometer (Lambda 950) equipped with an integrating sphere. Photocurrent measurements were conducted in a typical three electrode electrochemical system (CHI-660D), under visible light illumination (Xenon lamp,  $100 \text{ mW cm}^{-2}$ ,  $\lambda > 420 \text{ nm}$ ) at zero bias versus saturated calomel electrode (SCE).

Photocatalytic water splitting experiments were conducted in a 500 ml cylinder quartz reactor at ambient temperature. A 300 W xenon lamp with a simulated sunlight filter (light intensity was  $100 \text{ mW cm}^{-2}$ ) used as a light source. The prepared photocatalyst was placed on the bottom of reactor containing 100 ml mixed aqueous solution with 3.15 g  $\text{Na}_2\text{SO}_3$  and 8.4 g  $\text{Na}_2\text{S}$ . A certain amount of gas was intermittently sampled and analyzed by gas chromatography (GC-14C, Shimadzu, Japan, thermal conductivity detector, nitrogen as a carrier gas, and  $5 \text{ \AA}$  molecular sieve column).

The FESEM image of the as-prepared  $\text{WS}_2$ -Au-CIS sample is shown in Fig. 1(a). As can be seen, the CF is entirely covered with the nanotubular material. Accordingly, Fig. 1(b) depicts the EDX spectrum taken from a micro area of the  $\text{WS}_2$ -Au-CIS sample. It reveals a Cu/In atomic ratio of close to 1:1 suggesting the electrochemical reaction of  $\text{Cu}^{2+}$  and  $\text{In}^{3+}$  takes place in one step without the formation of any intermediate phase. TEM of single tube  $\text{WS}_2$ -Au-CIS is presented in Figs. 1(c) and 1(d). The obvious lattice fringes with a spacing of 0.62 nm can be indexed to the (002) plane of hexagonal  $\text{WS}_2$  (ICDD, No. 35-0651). It is evident from the HRTEM image that the hemispherical core-shell type nanoparticles formed on to  $\text{WS}_2$  nanotube having diameter and thickness of 100 nm and 5–10 nm, respectively. The lattice spacing of the core was determined to be 0.20 nm, which is in agreement with the cubic Au (200) plane (ICDD, No. 04-0784), and the

0.32 nm spacing of the shell can be attributed to the tetragonal CIS (112) plane (ICDD, No. 27-0159).

Raman spectra were obtained by 532 nm laser in back-scattering geometry and illustrated in Fig. 2(a). The Raman spectrum of  $\text{WO}_3$  nanowires disappeared as a comparison to prove the complete sulfurization. The CIS is characterized by its particular longitudinal phonon mode at  $290 \text{ cm}^{-1}$ .<sup>33</sup> This feature endured in  $\text{WS}_2$ -Au-CIS reveals the constituent of CIS in the target material. Furthermore, the band centered at  $418 \text{ cm}^{-1}$  and  $350 \text{ cm}^{-1}$  is attributed to W-S stretching from the  $\text{WS}_2$  nanotube.<sup>34</sup> The crystallographic information was obtained from XRD pattern (Fig. 2(b)). Besides the dominant peak of CF (002) (ICDD, No. 41-1487), three sets of typical diffraction signals for each of  $\text{WS}_2$ , Au, and CIS can be identified. Consequently, the reflection at  $14.3^\circ$  is indexed to the plane (002) of the  $\text{WS}_2$  (ICDD, No. 35-0651). The planes (004) and (006) are also meant for  $\text{WS}_2$ . The peak near the CF (002) can be attributed to the (112) plane of CIS. Although very weak, due to its low amount, the characteristic features of Au corresponding to (111), (200), and (220) planes can still be identified.

Diffusive reflectance absorption spectra (400 nm–1000 nm) of the samples were also measured (Fig. 2(c)). The peaks at 525 nm for  $\text{WS}_2$ -Au and  $\text{WS}_2$ -Au-CIS samples represent efficient light absorption caused by the localized surface plasmonic resonance (LSPR) of the Au nanoparticles.<sup>35</sup>  $\text{WS}_2$ -Au-CIS, as compared to  $\text{WS}_2$ -CIS, shows a significantly intensified absorption in the visible region only due to the SPR effect of Au nanoparticles. Moreover, the peak at 620 nm belongs to the  $\text{WS}_2$  nanotube, which is also apparent from the yellowish appearance of the CF.<sup>18</sup> The CIS sample exhibits typical semiconductor absorption spectra.

For further theoretical insight into our photocatalytic system, we modeled the  $\text{WS}_2$ -Au-CIS with software of Comsol

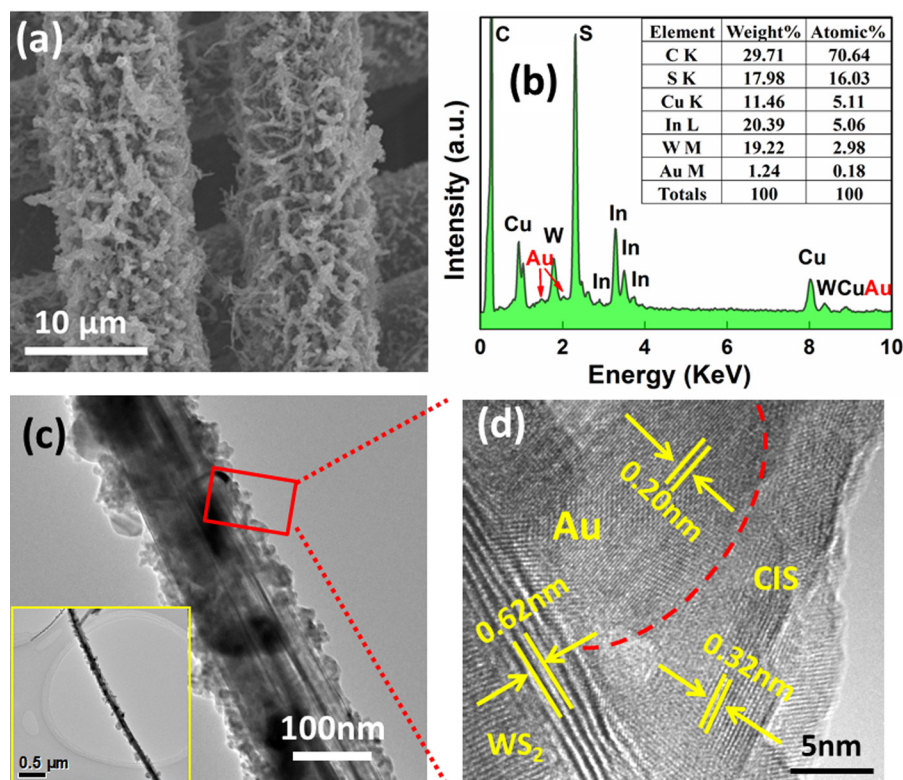


FIG. 1. (a) SEM image and (b) EDX spectrum of  $\text{WS}_2$ -Au-CIS sample on carbon fiber, (c) TEM image of a single  $\text{WS}_2$ -Au-CIS. Inset is a low magnification TEM image. (d) HRTEM image of  $\text{WS}_2$ , CIS, and Au.

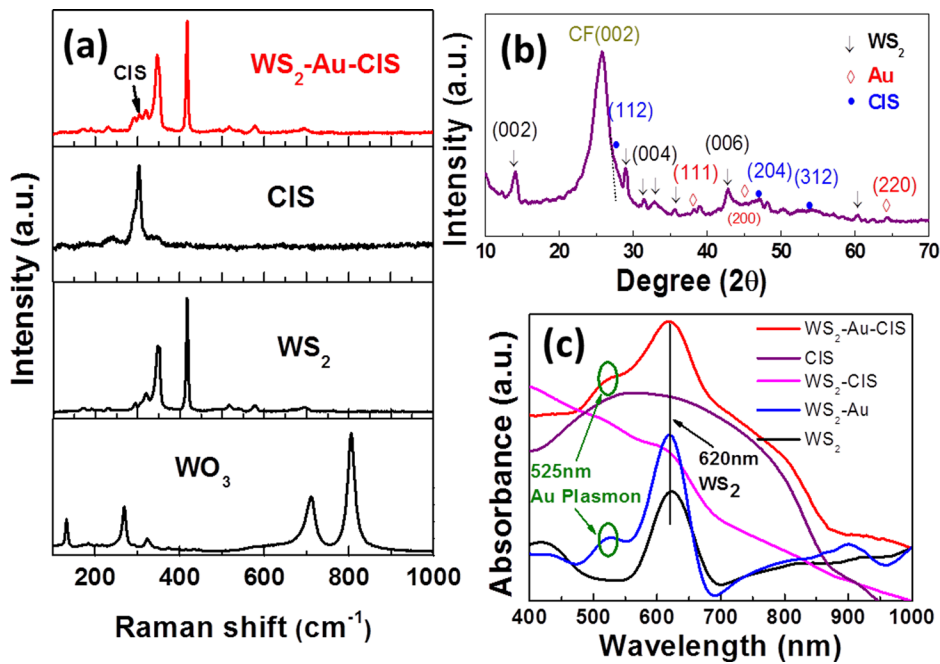


FIG. 2. (a) Raman spectra of WO<sub>3</sub>, WS<sub>2</sub>, CIS, and WS<sub>2</sub>-Au-CIS. (b) XRD pattern of WS<sub>2</sub>-Au-CIS. (c) Diffusive reflectance absorption spectra (from 400 nm to 1000 nm) of the samples.

Multi physics. The inset of Fig. 3(a) describes a model, in which Au nanoparticles attach on the side of WS<sub>2</sub> and are surrounded by CIS. The diameter of WS<sub>2</sub> tube is 100 nm, thickness of the CuInS<sub>2</sub> is 5 nm, and the diameter of Au nanoparticle is 20 nm. The refractive index of the surrounding water was taken to be 1.33. The Au dielectric function was represented by fitting the data points from Ref. 36.

Up on illumination of light on the Schottky barrier, the surface plasmons of the metal nanoparticles will decay into highly energetic “hot” electrons, thereby transported to the metal-semiconductor interface and injected into the conduction band of the semiconductor. This process can be understood by

a simple model,<sup>37</sup> in which the amount of the hot electrons  $A(\nu)$  can be written as an expression with the quantum transmission probability  $\eta_i$  modified by the plasmon absorption spectrum  $S(\nu)$

$$A(\nu) = \eta_i S(\nu) = C_F \frac{(h\nu - q\Phi_B)^2}{h\nu} S(\nu), \quad (1)$$

where  $C_F$  is the device-specific Fowler emission coefficient,  $h\nu$  is the photon energy, and  $q\Phi_B$  is the Schottky barrier energy. The quantum transmission probability  $\eta_i$  describes the number of electrons with sufficient energy to overcome the potential barrier. A finite element method (FEM) is used

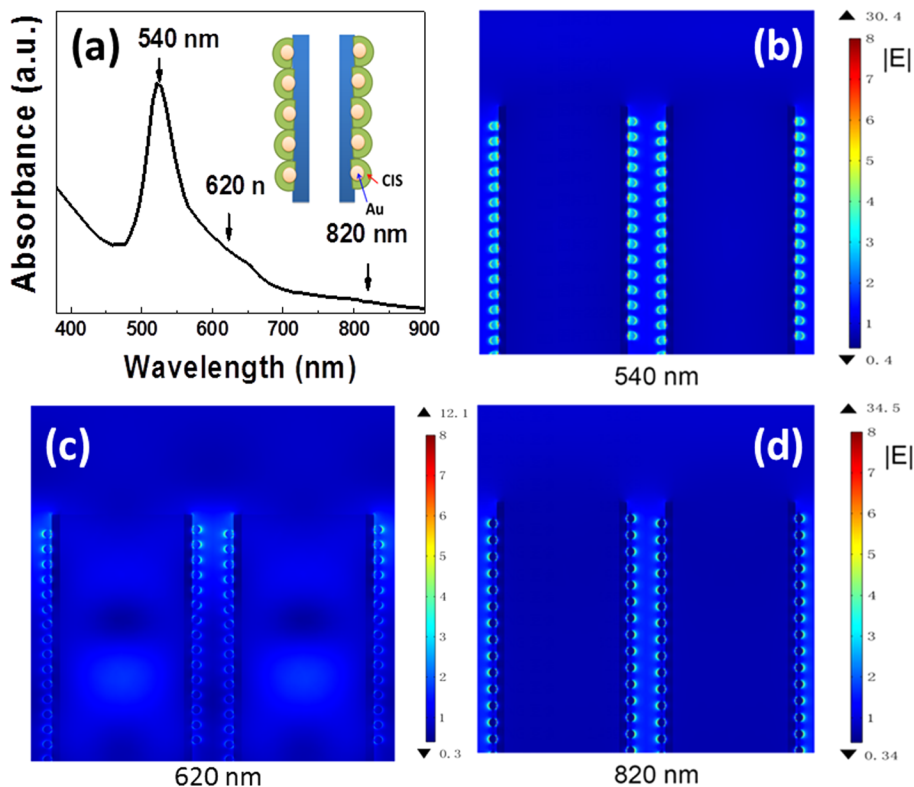


FIG. 3. (a) The absorption cross section spectrum for a single Au nanoparticles immersed in water. The inset is a model of WS<sub>2</sub>-Au-CIS structure. And the electric field distributions of the WS<sub>2</sub>-Au-CIS sample at the wavelengths of (b) 540 nm, (c) 620 nm, and (d) 820 nm.



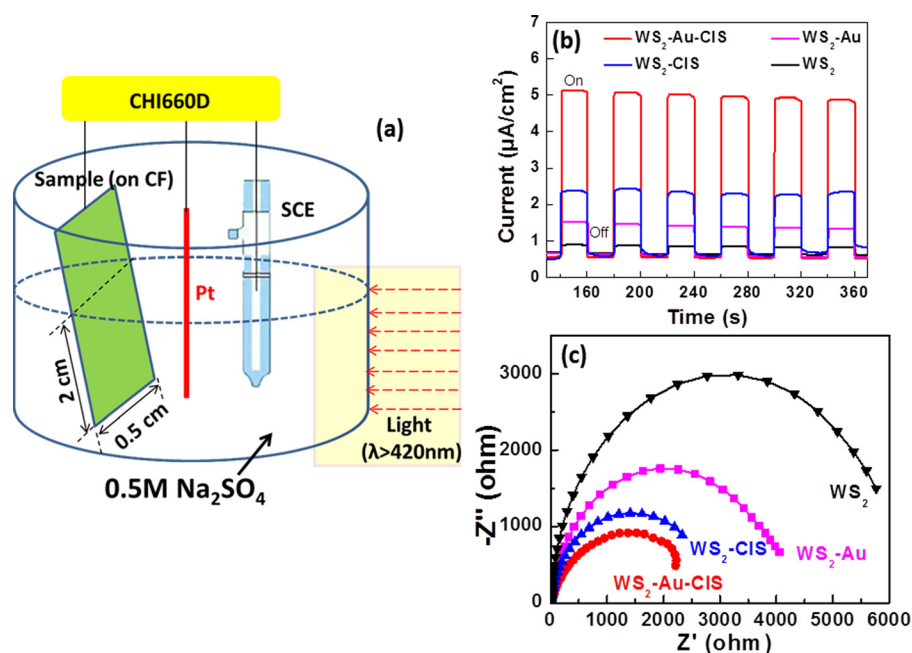


FIG. 4. (a) Schematic drawing of the PEC setup. (b) The time course photocurrent responses of sample electrodes with visible light on/off at zero bias versus SCE. (c) EIS plots of sample electrodes under open-circuit potential under the light. Light: Xenon lamp,  $100 \text{ mW cm}^{-2}$ ,  $\lambda > 420 \text{ nm}$ .

to simulate the absorption spectrum. Due to the strong plasmon resonance of the Au nanoparticles, the other surrounding materials, such as water, WS<sub>2</sub>, and CIS, only give a small frequency shift for nanoparticle plasmon resonances.<sup>38</sup> As shown in Fig. 3(a), the maximal absorption is located at about 540 nm, which corresponds to the LSPR effect of the Au nanoparticles. From Figs. 3(b)–3(d), the magnitude of the electric field around the nanoparticles at the localized SPR wavelength 540 nm is the strongest. According to Eq. (1), at 540 nm, since the nanoparticle absorbs appreciable amount of light, and the generated hot electrons will thus have sufficient energy to overcome the potential barrier resulting in the highest efficiency of hydrogen production, which agrees with the following experimental data very well.

Fig. 4(a) shows a schematic drawing of the PEC measurement setup. The active area of all samples is  $0.5 \text{ cm} \times 2 \text{ cm} = 1 \text{ cm}^2$ . Samples are used as cathode and counter electrode is Pt. The time course photocurrent responses of sample electrodes with visible light on/off are depicted in Fig. 4(b). It is evident that the WS<sub>2</sub> exhibits a lowest photocurrent (Fig. 4(b), black line) accompanied by a biggest arc radius in electrochemical impedance spectra (EIS) Nyquist plots (Fig. 4(c), black line) due to its faint light response and inefficient separation of charge carrier. The incorporation of Au nanoparticles on WS<sub>2</sub> leads to the increase of photocurrent under visible light irradiation because of the generation of hot electrons by the Au plasmon (Fig. 4(b), pink line). Interestingly, the

deposition of CIS on WS<sub>2</sub> further improves the response and diminishes the EIS circle as a result of the type-II configuration between WS<sub>2</sub> and CIS. It is also apparent that WS<sub>2</sub>-Au-CIS displays the boosted photocurrent response and efficient carrier separation (Figs. 4(b) and 4(c), red line), which would play an important role in the efficacy of water splitting.

The hydrogen generation experiments for different samples were carried in an aqueous solution containing Na<sub>2</sub>S and Na<sub>2</sub>SO<sub>3</sub> under visible light irradiation (Fig. 5(a)). Mass loading of WS<sub>2</sub>-Au-CIS is around  $1.5 \text{ mg}/\text{cm}^2$ . Other samples have a little difference. As anticipated, there is no observable H<sub>2</sub> generation from the WS<sub>2</sub>-Au and WS<sub>2</sub>-CIS-Au samples. This may be due to the conductive band edge of WS<sub>2</sub> is below the H<sup>+</sup> redox potential at current pH ( $\sim 10$ ). For WS<sub>2</sub>-CIS-Au, the shielding Au keeps the WS<sub>2</sub>-CIS away from the water. The photocurrent of WS<sub>2</sub>-CIS type-II structure is enhanced, but the H<sub>2</sub> generation rate still remains unsatisfactory because of the fact that the electrons thermodynamically prefer to move from the conductive band (CB) of CIS to that of WS<sub>2</sub>. It is interesting that the WS<sub>2</sub>-Au-CIS sample demonstrates the highest H<sub>2</sub> yield among all samples. In addition, it is obviously observed that Au/CIS, CIS, and CIS/Au demonstrate obviously different H<sub>2</sub> production rates. CIS can photocatalyze H<sub>2</sub>O to produce H<sub>2</sub>, which is contributed to its suitable band structure. Au/CIS can generate a little more H<sub>2</sub> than CIS, which is due to the Au LSPR effects. In contrast, CIS/Au significantly decreases H<sub>2</sub> production

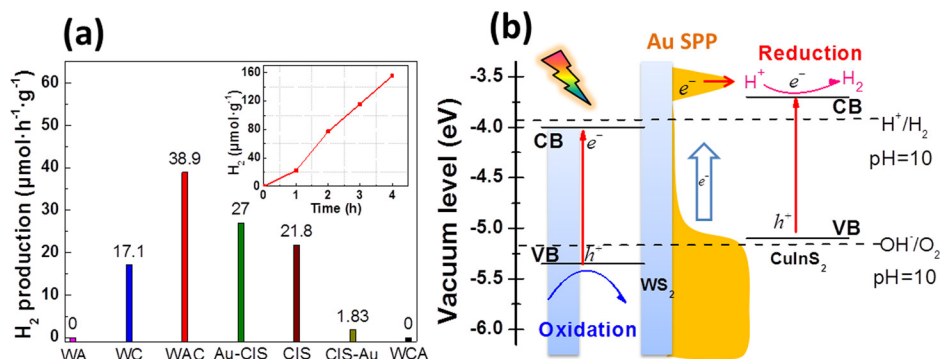


FIG. 5. (a) H<sub>2</sub> production for WS<sub>2</sub>-Au (WA), WS<sub>2</sub>-CIS (WC), WS<sub>2</sub>-Au-CIS (WAC), Au-CIS, CIS, CIS-Au, and WS<sub>2</sub>-CIS-Au (WCA). The inset is the H<sub>2</sub> production plot of WS<sub>2</sub>-Au-CIS. (b) A tentative mechanism scheme.

rate than both CIS and Au/CIS. This may be because the outer Au nanoparticles keep the catalyst CIS out of the water.

A tentative electron transport mechanism was proposed for the sandwiched structure of WS<sub>2</sub>-Au-CIS (Fig. 5(b)). The band energy data of WS<sub>2</sub> and CIS are obtained from previous literatures.<sup>11,25,39</sup> Considering the solution pH is 10, we calculate the E(H<sup>+</sup>/H<sub>2</sub>) and E(OH<sup>-</sup>/O<sub>2</sub>) at pH 10 according to Nernst equation. Under the visible light, the Au nanoparticles introduce the LSPR effects allowing the transport of high energy electrons from the Au nanoparticle to the CB of CIS. Additionally, the photogenerated electrons of WS<sub>2</sub> can transfer to the Au nanoparticles because of the higher vacuum energy level compared with the Fermi level (E<sub>F</sub>) of the Au. Another process, so-called vectorial electron transfer scheme,<sup>35</sup> may also occur in this WS<sub>2</sub>-Au-CIS structure, in which the photoelectrons from the CB of WS<sub>2</sub> transfer to the VB of CIS via the Au nanoparticle. While it indicates that the Au plasmonic effect is evidenced from the paramount yield of H<sub>2</sub>, which has no structure to form the vectorial electron transfer scheme. So we prefer that the Au plasmonic effect produced more high energy electrons to enhance the H<sub>2</sub> production, instead of the vectorial electron transfer scheme.<sup>28</sup> In general, the plasmon Au nanoparticles transport the electrons to the conduction band of the CIS liking a pump, which were excited by light from the VB to the CB of the WS<sub>2</sub>. Without the Au nanoparticles, the type-II structure would be formed between WS<sub>2</sub> and CIS. Thus, the photocurrent of this structure may be enhanced, while the H<sub>2</sub> generation rate must be decreased because of the fewer active electrons. With the plasmon Au nanoparticles, an electron transport process in reverse was established between WS<sub>2</sub> and CIS compared to the type-II structure.

In summary, we have developed an efficient WS<sub>2</sub>-Au-CIS photocatalyst by loading Au nanoparticles first and then CIS nanoparticles onto CVD-synthesized WS<sub>2</sub> nanotubes for hydrogen production. From diffusive reflectance absorption spectra, it can be seen that Au nanoparticles show significant surface plasmonic resonance peak at 525 nm, which leads to the significant enhancement of the light absorption in comparison with the samples without Au. The PEC measurements show the WS<sub>2</sub>-Au-CIS photocatalysts own enhanced photo absorption and photo current response. Further, the hydrogen generation experiments depict WS<sub>2</sub>-Au-CIS photocatalysts have the highest efficiency of hydrogen production. These results should be attributed to the faster photogenerated carrier separation from the type II band structures and the LSPR effect from the Au nanoparticles. Our findings can provide an efficient method to further promote the photocatalyst performance of type-II structures by introducing SPR effects from metal nanoparticles.

This work was supported by the National Natural Science Foundation of China (Nos. 21373065 and 61474033), 973 Program of the Ministry of Science and Technology of China (No. 2012CB934103), Beijing Natural Science Foundation (No. 2144059), and CAS Key Laboratory of Nanosystem and Hierarchical Fabrication. The authors gratefully acknowledge the support of K. C. Wong Education Foundation.

- <sup>1</sup>A. Kudo and Y. Miseki, *Chem. Soc. Rev.* **38**, 253–278 (2009).
- <sup>2</sup>K. Maeda, *ACS Catal.* **3**, 1486–1503 (2013).
- <sup>3</sup>P. Zhou, J. Yu, and M. Jaroniec, *Adv. Mater.* **26**, 4920–4935 (2014).
- <sup>4</sup>K. Iwashina, A. Iwase, Y. H. Ng, R. Amal, and A. Kudo, *J. Am. Chem. Soc.* **137**, 604–607 (2015).
- <sup>5</sup>R. Kobayashi, S. Tanigawa, T. Takashima, B. Ohtani, and H. Irie, *J. Phys. Chem. C* **118**, 22450–22456 (2014).
- <sup>6</sup>H. J. Yun, H. Lee, N. D. Kim, D. M. Lee, S. Yu, and J. Yi, *ACS Nano* **5**, 4084–4090 (2011).
- <sup>7</sup>T. T. Hong, Z. F. Liu, W. G. Yan, B. Wang, X. Q. Zhang, J. Q. Liu, J. K. Wang, and J. H. Han, *Chem. Commun.* **51**, 13678–13681 (2015).
- <sup>8</sup>Y. Wang, Q. Wang, X. Zhan, F. Wang, M. Safdar, and J. He, *Nanoscale* **5**, 8326–8339 (2013).
- <sup>9</sup>J. H. Han, Z. F. Liu, K. Y. Guo, B. Wang, X. Q. Zhang, and T. T. Hong, *Appl. Catal., B* **163**, 179–188 (2015).
- <sup>10</sup>M. L. Tang, D. C. Grauer, B. Lassalle-Kaiser, V. K. Yachandra, L. Amirav, J. R. Long, J. Yano, and A. P. Alivisatos, *Angew. Chem., Int. Ed.* **50**, 10203–10207 (2011).
- <sup>11</sup>W. K. Ho, J. C. Yu, J. Lin, J. G. Yu, and P. S. Li, *Langmuir* **20**, 5865–5869 (2004).
- <sup>12</sup>J. Ran, J. Zhang, J. Yu, M. Jaroniec, and S. Z. Qiao, *Chem. Soc. Rev.* **43**, 7787–7812 (2014).
- <sup>13</sup>H. Tributsch, *Ber. Bunsen-Ges.-Phys. Chem. Chem. Phys.* **81**, 361–369 (1977).
- <sup>14</sup>X. Zong, J. Han, G. Ma, H. Yan, G. Wu, and C. Li, *J. Phys. Chem. C* **115**, 12202–12208 (2011).
- <sup>15</sup>G. Chen, F. Li, Y. Fan, Y. Luo, D. Li, and Q. Meng, *Catal. Commun.* **40**, 51–54 (2013).
- <sup>16</sup>S. Bassaid, B. Bellal, and M. Trari, *React. Kinet., Mech. Catal.* **115**, 389–400 (2015).
- <sup>17</sup>A. DiPaola, L. Palmisano, M. Derrigo, and V. Augugliaro, *J. Phys. Chem. B* **101**, 876–883 (1997).
- <sup>18</sup>K. Xu, F. Wang, Z. Wang, X. Zhan, Q. Wang, Z. Cheng, M. Safdar, and J. He, *ACS Nano* **8**, 8468–8476 (2014).
- <sup>19</sup>R. Scheer, T. Walter, H. W. Schock, M. L. Fearheiley, and H. J. Lewerenz, *Appl. Phys. Lett.* **63**, 3294 (1993).
- <sup>20</sup>I. Tsuji, H. Kato, and A. Kudo, *Angew. Chem., Int. Ed.* **117**, 3631–3634 (2005).
- <sup>21</sup>S. Ikeda, T. Nakamura, S. M. Lee, T. Yagi, T. Harada, T. Minegishi, and M. Matsumura, *ChemSusChem* **4**, 262–268 (2011).
- <sup>22</sup>Y. Lin, F. Zhang, D. Pan, H. Li, and Y. Lu, *J. Mater. Chem.* **22**, 8759 (2012).
- <sup>23</sup>K. Guo, Z. Liu, J. Han, Z. Liu, Y. Li, B. Wang, T. Cui, and C. Zhou, *Phys. Chem. Chem. Phys.* **16**, 16204–16213 (2014).
- <sup>24</sup>C. Li, Z. Xi, W. Fang, M. Xing, and J. Zhang, *J. Solid State Chem.* **226**, 94–100 (2015).
- <sup>25</sup>T. L. Li, C. D. Cai, T. F. Yeh, and H. Teng, *J. Alloys Compd.* **550**, 326–330 (2013).
- <sup>26</sup>Y. Li, Z. Liu, Y. Wang, Z. Liu, J. Han, and J. Ya, *Int. J. Hydrogen Energy* **37**, 15029–15037 (2012).
- <sup>27</sup>X. Wang, S. Li, Y. Ma, H. Yu, and J. Yu, *J. Phys. Chem. C* **115**, 14648–14655 (2011).
- <sup>28</sup>S. Linic, P. Christopher, and D. B. Ingram, *Nat. Mater.* **10**, 911–921 (2011).
- <sup>29</sup>A. J. van der Vlies, R. Prins, and T. Weber, *J. Phys. Chem. B* **106**, 9277–9285 (2002).
- <sup>30</sup>Y. Zheng, X. Zhong, Z. Li, and Y. Xia, *Part. Part. Syst. Charact.* **31**, 266–273 (2014).
- <sup>31</sup>J. H. Yun, Y. H. Ng, S. Huang, G. Conibeer, and R. Amal, *Chem. Commun.* **47**, 11288–11290 (2011).
- <sup>32</sup>S. Vadivel, K. Srinivasan, and K. R. Murali, *Mater. Sci. Semicond. Process.* **16**, 765–770 (2013).
- <sup>33</sup>M. Nanu, J. Schoonman, and A. Goossens, *Adv. Funct. Mater.* **15**, 95–100 (2005).
- <sup>34</sup>A. Berkdemir, H. R. Gutiérrez, A. R. Botello-Méndez, N. Perea-López, A. L. Elías, C.-I. Chia, B. Wang, V. H. Crespi, F. López-Urías, J.-C. Charlier, H. Terrones, and M. Terrones, *Sci. Rep.* **3**, 1755 (2013).
- <sup>35</sup>H. Tada, T. Mitsui, T. Kiyonaga, T. Akita, and K. Tanaka, *Nat. Mater.* **5**, 782–786 (2006).
- <sup>36</sup>P. B. Johnson and R. W. Christy, *Phys. Rev. B* **6**, 4370–4379 (1972).
- <sup>37</sup>M. W. Knight, H. Sobhani, P. Nordlander, and N. J. Halas, *Science* **332**, 702–704 (2011).
- <sup>38</sup>S. Mubeen, G. Hernandez-Sosa, D. Moses, J. Lee, and M. Moskovits, *Nano. Lett.* **11**, 5548–5552 (2011).
- <sup>39</sup>F. Yang, V. Kuznietsov, M. Lublow, C. Merschjann, A. Steigert, J. Klaer, A. Thomas, and T. Schedel-Niedrig, *J. Mater. Chem. A* **1**, 6407–6415 (2013).